



# Politecnico di Bari

Repository Istituzionale dei Prodotti della Ricerca del Politecnico di Bari

A finite element method for a weakly nonlinear dynamic analysis and bifurcation tracking of thermo-acoustic instability in longitudinal and annular combustors

This is a pre-print of the following article

*Original Citation:*

A finite element method for a weakly nonlinear dynamic analysis and bifurcation tracking of thermo-acoustic instability in longitudinal and annular combustors / Laera, Davide; Campa, Giovanni; Camporeale, Sergio Mario. - In: APPLIED ENERGY. - ISSN 0306-2619. - 187:(2017), pp. 216-227. [10.1016/j.apenergy.2016.10.124]

*Availability:*

This version is available at <http://hdl.handle.net/11589/106534> since: 2022-06-06

*Published version*

DOI:10.1016/j.apenergy.2016.10.124

*Terms of use:*

(Article begins on next page)

# A finite element method for a weakly nonlinear dynamic analysis of thermo-acoustic instability in longitudinal and annular combustors

D. Laera<sup>a,\*</sup>, G. Campa<sup>b</sup>, S.M. Camporeale<sup>a</sup>

<sup>a</sup>*Politecnico di Bari, 70125 Via Re David, 200, Bari (Ba), Italy*

<sup>b</sup>*Product Development Turbomachinery and Combustion, Ansaldo Sviluppo Energia S.r.l, 16152, Genova, Italy*

---

## Abstract

Low-frequency nonlinear dynamics of thermo-acoustic modes in longitudinal and annular combustors have been intensively studied experimentally, numerically, and theoretically to better understand the mechanisms leading to limit cycles. This article presents a numerical procedure based on a finite element method able to perform weakly nonlinear analysis of longitudinal as well as multi-burner annular combustors considering complex nonlinear flame models. At first the proposed numerical procedure is validated in a longitudinal configuration against analytical results obtained in a low-order framework, nonlinear flame models with a third-order and of a fifth-order polynomial with time delays are assumed. Subsequently, the ability of the proposed numerical approach to treat complex combustion systems with independent flames is verified on an annular configuration equipped with twelve burners. In both configurations, at the variation of the acoustic-combustion interaction index  $n$ , the amplitudes of velocity fluctuations of the predicted

---

\*Corresponding author: [davide.laera@poliba.it](mailto:davide.laera@poliba.it)

limit cycles are plotted against the control parameter to track the bifurcation diagrams. Regardless of the configuration, supercritical and subcritical bifurcations are obtained depending of the chosen flame model. In a second step, the influence on the bifurcation trajectories of the time delay and of the amount of acoustic damping is investigated. Results reveal an influence of both parameters on the position of the Hopf bifurcation points and of the fold points and also an impact on the limit cycle amplitude of the velocity fluctuations.

*Keywords:* Thermo-acoustic instabilities, Helmholtz solver, Longitudinal combustor, Annular combustor, Limit cycles, Bifurcation diagrams

---

## 1. Introduction

1 Lean premixed combustors used in modern gas turbines for power genera-  
2 tion and aero-engines are often affected by combustion instabilities generated  
3 by mutual interactions between pressure fluctuations ( $p'$ ) and heat release  
4 rate oscillations ( $\dot{q}'$ ) produced by the flame [1, 2, 3]. Many theoretical and  
5 numerical studies are focused on the analysis of limit cycles of low-frequency  
6 instabilities considering simple longitudinal configurations assuming theoret-  
7 ical flame response models [4, 5, 6, 7]. The main difficulty to perform these  
8 analyses is the definition of the model used to describe the response of the  
9 flame to acoustic perturbations [8]. If a linear response is assumed, a sta-  
10 bility analysis can be performed in order to identify the frequency at which  
11 the system is unstable meaning that pressure oscillations may start after in-  
12 finitesimally small disturbances [9, 10, 11, 12]. However, linear tools cannot  
13 account for finite amplitude effects on the oscillation frequency and cannot

14 predict the fluctuations level. These features can be examined by combining  
15 an acoustic model of the system with a nonlinear description of the flame  
16 dynamics [13, 7]. The evaluation of a suitable nonlinear flame model for a  
17 given combustor is, probably, one of the most challenging task of the study of  
18 thermo-acoustic combustion instability. In annular configurations more diffi-  
19 culties arise due to the presence of multiple flames which respond collectively  
20 over a wide frequency range [14]. The present study deals with these difficul-  
21 ties developing a numerical approach able to perform limit cycle calculations  
22 considering complex nonlinear flame models with time delays in combina-  
23 tion with a Helmholtz solver, using this framework to calculate the limit  
24 cycle conditions and the bifurcation diagrams of a single burner longitudinal  
25 combustor and of a more complex multi-burner annular configuration.

26 At this point, it is worth briefly reviewing some recent investigations  
27 of nonlinear flame models. First studies on the transition to the limit cycle  
28 were carried out in solid fuel rocket motors by Culick who observed that some  
29 stable motors would suddenly jump to a self-sustained oscillation state, when  
30 pulsed [15]. Since in rocket engines the oscillations have such high amplitudes  
31 that the gas dynamics is nonlinear, he considered nonlinear gas dynamics  
32 and linear flame models. Nonlinear combustion models were later taken into  
33 account [16], assuming that the heat release rate was a quadratic or rectified  
34 (modulus sign) function of the fluctuating velocity or pressure.

35 The bifurcation diagram can be helpful for understanding the influence  
36 of nonlinear flame model, since it shows the amplitude of limit cycles as a  
37 function of control parameters. This is useful if there is a known bound  
38 on the acceptable oscillation amplitude. It also shows whether the point

39 of linear instability (the so called Hopf bifurcation point) is supercritical  
40 or subcritical. This is an important qualitative distinction because: in a  
41 subcritical system, high amplitude oscillations occur suddenly when the state  
42 becomes linearly unstable and even when the system is linearly stable; in a  
43 supercritical system, amplitude oscillations occur only when the system is  
44 linearly unstable [17].

45 In the years several techniques have been proposed in order to track  
46 the bifurcation diagrams. Due to the complexity of the problem most of  
47 them deals with longitudinal combustor characterized by one single source  
48 of heat release rate. Subcritical bifurcation is obtained by Moeck *et al.* [18]  
49 performing a systematic variation of parameters and tracking direct time  
50 integration. However this method is computationally expensive.

51 Another method for obtaining the bifurcation diagrams is numerical con-  
52 tinuation [16, 19, 20]. This approach is based on the iterative solution of a  
53 set of parameterized nonlinear equations given an initial guess. The diagram  
54 is tracked varying a parameter and including the solutions which satisfy the  
55 set of equations for a given state of the system. The unstable limit cycle can  
56 also be computed. Compared to other methods, it is very efficient in obtain-  
57 ing the dependence of the solution from the control parameter. However,  
58 it takes a long time to map the bifurcation diagram and it can be also too  
59 computationally expensive. Thanks to improvements in the method and in  
60 the parallel computing, continuation methods are likely to become important  
61 tools in nonlinear analysis of thermo-acoustics [21].

62 Juniper [21] and Subramanian *et al.* [22] used DDE-BIFTOOL, which is a  
63 software based on the numerical continuation methods for delay systems [23].

64 The steady state of the system is evaluated through the Newton-Raphson  
65 scheme and the steady state solution is used for tracking the bifurcation di-  
66 agram as the control parameter varies. The use of low-order network models  
67 to map the bifurcation diagram as a function of a control parameter has  
68 been shown by Campa and Juniper [24]. Instead of numerically integrate the  
69 fully non-linear equations governing the phenomenon, the authors proposed  
70 a weakly nonlinear approach consisting in a linear eigenvalue analysis around  
71 a non-linear steady state of the system. This approach, less computationally  
72 expensive than the continuation method, will be used in this work. Subra-  
73 manian *et al.* [5] has analyzed subcritical transition to instability relating  
74 the non-linearity in the model with the criticality of the ensuing bifurca-  
75 tion, starting from the equation of Stuart-Landau. They also identify the  
76 parameter regions where triggering is possible using the method of harmonic  
77 balance.

78 The Flame Describing Function (FDF) approach was developed to re-  
79 produce the limit cycles experimentally observed [25]. The stability map  
80 of a burner with an unconfined flame [26] and of a burner with a confined  
81 flame [27, 28] was obtained by using flame describing functions. Recently this  
82 methodology was applied to the case of turbulent premixed swirled flames  
83 [7, 29]. Additionally, a diffusion flame characterizing a Rijke tube has been  
84 modeled by means of flame describing function to get the stability map [30].  
85 Nonlinear effects induced by nonstandard types of fluctuations in a multiple  
86 flame combustor equipped with a perforated plate were investigated by Kabi-  
87 raj *et al.* [31]. Very recently, Heckl [32] has modeled the measured Flame  
88 Describing Function by Noiray *et al.* [26] with an entirely analytical approach,

89 finding the pattern of the oscillation regimes in parameter space, such as fre-  
90 quency and amplitude of limit cycles at different conditions. However, it  
91 should be notice that a FDF does not provide only the flame response of a  
92 specific combustor but is also a description of the entire burner area, includ-  
93 ing the effects of flame confinement, heat losses and interaction of the flame  
94 with the walls, all aspects that make the FDF linked to the specific combustor  
95 and operating conditions at which the measurements are performed.

96 Very few are the works in which a nonlinear analysis is performed on  
97 an annular combustor. The problem may be simplified by considering only  
98 one single azimuthal mode described by Van der Pol oscillator equations  
99 coupled with a nonlinear flame model expressed in terms of pressure pertur-  
100 bation. Results in [33, 34, 35] indicate that this approach is able to predict  
101 both spinning and standing unstable modes depending on the nonlinearity  
102 and nonuniformity in the flame response. Recently, Bourgouin *et al.* [36]  
103 managed to introduce in their analytical one-dimensional framework a more  
104 reliable experimental Flame Describing Function (FDF) however the heat re-  
105 lease rate from the different burners is considered uniformly distributed over  
106 the circumference of the annular chamber. Following this approach, the spin-  
107 ning instability recorded during experiments of the laboratory scale MICCA  
108 annular combustor was reproduced in terms of frequency and amplitude of  
109 velocity fluctuations at the limit cycle. Multiple independent flames are con-  
110 sidered in the acoustic network modeling approach developed by Parmentier  
111 *et al.* [37] followed by Bauerheim *et al.* [38]. They presented however, only  
112 a linear stability analysis of spinning and standing modes assuming a sim-  
113 ple time delay  $n\tau$  dynamical response. Three dimensional geometries may

114 be analyzed by means a Helmholtz solver approach. In the time domain  
115 Pankiewicz and Sattelmayer [39], examined a three-dimensional combustion  
116 chamber, predicting the amplitude of limit cycles determined by a nonlinear  
117 flame model with a very simple saturation mechanism. Campa and Cam-  
118 poreale [10, 40] performed a linear stability analysis of a practical annular  
119 combustor assuming a distributed flame transfer function. On the compu-  
120 tational level, Large-Eddy Simulation (LES) codes have been used to inves-  
121 tigate combustion instability by suitably calculating pressure oscillations in  
122 combination with turbulent combustion phenomena [41, 42]. Large numerical  
123 resources are, however, required.

124 The present article specifically reports a numerical technique able to per-  
125 form a weakly nonlinear analysis of thermo-acoustic combustion instabilities  
126 in a Helmholtz solver framework. In the frequency domain, the limit cycle  
127 condition, i.e. the condition in which the growth rate  $\alpha$  equals zero, is pre-  
128 dicted solving the damped inhomogeneous Helmholtz equation coupled with  
129 two theoretical nonlinear flame models derived multiplying a linear  $n$ - $\tau$  flame  
130 transfer function (FTF) with a third-order and fifth-order polynomial expres-  
131 sion which saturate the gain of the FTF with the increase of the amplitude  
132 of velocity fluctuations  $|\hat{u}/\bar{u}|$ . At first the analysis is performed on a lon-  
133 gitudinal combustor. Varying the acoustic-combustion interaction index  $n$ ,  
134 the bifurcation diagrams are tracked assuming both nonlinear flame models.  
135 In a second step, for the first time, the analysis is conducted in an annular  
136 combustor with independent flames proving the feasibility of the presented  
137 numerical approach also for multiple flames configurations. In both configu-  
138 rations, the influence on the predicted limit cycles of the time delays and of



139 the damping level considered in the systems is also investigated. The article  
140 is organized as follow. After an overview of the nonlinear analysis theory  
141 presented in Section 2, the thermo-acoustic theory and the description of  
142 the flame models used in the study are presented in Section 3. Results are  
143 discussed in Section 4 for both configurations analyzed.

## 144 **2. Nonlinear analysis**

145 The behaviour of a nonlinear unstable system can change as a control  
146 parameter varies. These qualitative changes in the system dynamics are  
147 called bifurcations and the parameter values at which they occur is called  
148 bifurcation point [17].

149 Figure 1 shows two diagrams, describing the bifurcation dynamics as a  
150 function of a control parameter  $R$ . The variable on the y-axis is the steady  
151 state amplitude of the system, which is the limit cycle amplitude. At low  
152 values of  $R$  the system tends to a zero amplitude stable solution (solid line  
153 in Fig. 1). When  $R$  reaches the Hopf bifurcation point, the solution of the  
154 system becomes unstable. Increasing the value of the control parameter, the  
155 solution at zero amplitude remains unstable (dashed line in Fig. 1) and the  
156 system starts to oscillate reaching the steady state amplitude (solid line at  
157 non-zero amplitudes), known as the limit cycle or the stable periodic solution.

158

159 The nonlinear behavior around the Hopf bifurcation point determines two  
160 different types of bifurcation and how the system answers to nonlinear per-  
161 turbations. The first type is the supercritical bifurcation (Fig. 1a), which  
162 is characterized by a gradually increase of the amplitude once reached the

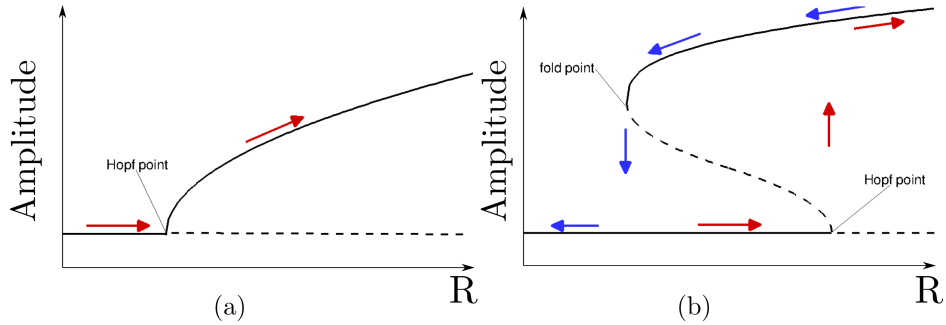


Figure 1: Steady state oscillation amplitude as a function of  $R$  for (a) a supercritical bifurcation and (b) a subcritical bifurcation [24]. As the control parameter  $R$  is increased, the system follows the red arrow path. As it is decreased, the system follows the blue arrow path.

163 Hopf point. In this condition, all perturbations imposed on the system tend  
 164 to decay to zero only if the Hopf point is not reached, otherwise all the per-  
 165 turbations reach a new stable periodic solution at the limit cycle equilibrium.  
 166 The second type of behavior is the subcritical bifurcation (Fig. 1b), which is  
 167 characterized by a sudden increase of the steady state amplitude at the Hopf  
 168 point. Once reached the limit cycle equilibrium, the perturbations imposed  
 169 on the system continue to reach a stable periodic solution even for values of  
 170  $R$  lower than the one corresponding to the Hopf point, until the fold point is  
 171 reached. For values of  $R$  lower than the one corresponding to the fold point,  
 172 all perturbations decay to zero, as shown by the blue arrow path in Fig. 1b.  
 173 The dashed line at non-zero amplitudes in Fig. 1b is known as the unsta-  
 174 ble periodic solution [17]. If the system is triggered to an amplitude below  
 175 the unstable periodic solution, the imposed perturbations tend to decay to  
 176 zero. Otherwise, the imposed perturbations tend to grow reaching the stable  
 177 periodic solution.

178 Considering the condition of a subcritical bifurcation as in Fig. 1b, the  
 179 behaviour of the growth rate as a function of the amplitude for a generic  
 180 value of the control parameter in the bi-stable zone is shown in Fig. 2. As  
 181 well described by Strogatz [17], two fixed points can be observed referring to  
 182 periodic solutions: the fixed point indicated with a full point refers to a stable  
 183 periodic solution, the fixed point indicated with a hollow point refers to an  
 184 unstable periodic solution. It can also be observed that if the derivative of the  
 185 growth rate to the amplitude at a constant control parameter is positive, the  
 186 fixed point is an unstable periodic solution. If the derivative of the growth  
 187 rate to the amplitude at a constant control parameter is negative, the fixed  
 point is a stable periodic solution.

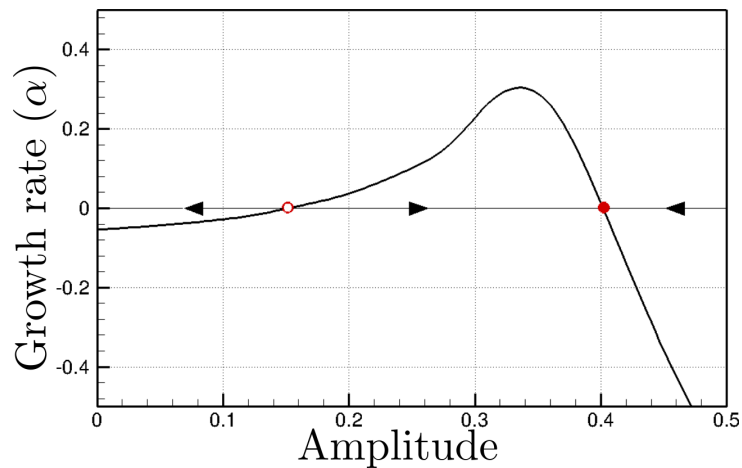


Figure 2: Growth rate ( $\alpha$ ) as a function of the amplitude for a generic value of the control parameter in the bistable zone, when a subcritical bifurcation occurs.

188

189 **3. The thermo-acoustic problem: Helmholtz solver approach**

190 The derivation of the mathematical model used for thermo-acoustic stud-  
 191 ies will be briefly discussed in this section. The complete formulation can be  
 192 found in other works [12, 43].

193 The fluid is regarded as an ideal gas. The effects of viscosity, thermal  
 194 diffusivity and heat transfer with walls are neglected, the mean pressure is  
 195 assumed uniform in the domain. The mean flow velocity  $\bar{u}$  is assumed much  
 196 lower than the speed of sound (hypothesis that is generally verified in the  
 197 combustion chamber of gas turbines [2]), so its influence on the propagation  
 198 of the pressure waves inside the duct is negligible. Under such hypotheses,  
 199 in presence of heat fluctuations, the inhomogeneous wave equation can be  
 200 obtained [12]

$$\frac{1}{c^2} \frac{\partial^2 p'}{\partial t^2} - \bar{\rho} \nabla \cdot \left( \frac{1}{\bar{\rho}} \nabla p' \right) = \frac{\gamma - 1}{c^2} \frac{\partial \dot{q}'}{\partial t}, \quad (1)$$

201 where  $p'$  is the pressure fluctuation,  $\dot{q}'$  is the heat release rate fluctuation  
 202 per unit volume,  $\gamma$  is the ratio of specific heats,  $\rho$  is the density and  $c$  is  
 203 the speed of sound. The effects of losses due to viscous and thermal bound-  
 204 ary layers can be modelled making use of suitable acoustic impedance as  
 205 boundary conditions. Here, aiming at analyzing the effects of damping, for  
 206 one dimensional combustion systems, the first derivative of  $p'$  in Eq. (1) is  
 207 multiplied by a nondimensional damping coefficient  $\zeta$  [44], giving

$$\frac{1}{c^2} \frac{\partial^2 p'}{\partial t^2} + \frac{\zeta}{c\mathcal{L}} \frac{\partial p'}{\partial t} - \bar{\rho} \nabla \cdot \left( \frac{1}{\bar{\rho}} \nabla p' \right) = \frac{\gamma - 1}{c^2} \frac{\partial \dot{q}'}{\partial t}, \quad (2)$$

208 where  $\mathcal{L}$  is the characteristic dimension of the analysed system. In this  
 209 work,  $\mathcal{L}$  is assumed equal to the radius in the longitudinal configuration

210 and to  $\sqrt{R_{ex}^2 - R_{in}^2}$  in case of the annular combustor, being  $R_{ex}$  and  $R_{in}$ ,  
 211 respectively, the external and the internal radius of the annulus domain in  
 212 which  $\zeta$  is considered. The damping coefficient for  $j^{th}$  mode is modelled as

$$\zeta_j = c_1 j^2 + c_2 j^{1/2} \quad (3)$$

213 where  $c_1$  and  $c_2$  are assumed constant for each mode. In this study, the  
 214 damping coefficients  $\zeta$  is varied from 0.03 to 0.3. More information on these  
 215 coefficients can be found in [45]. This is the only damping mechanism con-  
 216 sidered in this study. In all configurations analysed, either  $p'$  or  $u'$  are set  
 217 to zero at the boundaries of the computational domain, so that the energy  
 218 acoustic flux ( $f=p'\mathbf{u}'$ ) through the boundaries is null [43].

219 In the present article, the thermo-acoustic problem is solved in the fre-  
 220 quency domain. The fluctuating variables are expressed by complex functions  
 221 of time and position with a sinusoidal form:  $p'=\Re(\hat{p}\exp(i\omega t))$ , where  $\omega$  is a  
 222 angular frequency. Applying the harmonic analysis for  $p'$  and  $q'$  in Eq. (2)  
 223 the damped inhomogeneous Helmholtz equation is obtained in the frequency  
 224 domain

$$\frac{\lambda^2}{c^2}\hat{p} - \frac{\lambda\zeta}{c\mathcal{L}}\hat{p} - \bar{\rho}\nabla \cdot \left(\frac{1}{\rho}\nabla\hat{p}\right) = -\frac{\gamma-1}{c^2}\lambda\hat{q} \quad (4)$$

225 where  $\lambda = -i\omega$ . With the definition of the flame model, Eq. (4) yields a  
 226 classical linear stability problem at the eigenvalues  $\lambda$  [17]. In the eigenvalue  
 227 problem,  $\omega$  is a complex angular frequency, its real part gives the frequency of  
 228 the oscillations,  $f=\Re(\omega)/2\pi$  Hz, while the imaginary part of  $\omega$  corresponds  
 229 to the growth rate  $\alpha=-\Im(\omega)/2\pi$  s<sup>-1</sup> parameter that governs the stability  
 230 the system, considering that the damping is directly model in the solved  
 231 equations. If  $\alpha$  is positive, the acoustic mode is unstable so the amplitude of

232 fluctuations grows with time. If  $\alpha$  is negative, the acoustic mode is stable,  
 233 i.e., perturbations decay with time. A limit cycle condition is reached when  
 234  $\alpha=0$ .

### 235 3.1. The linear flame model

236 In the frequency domain, the linear flame model is assumed as the classical  
 237 n- $\tau$  model [2, 46]

$$\frac{\hat{q}}{\bar{q}} = -n \frac{\hat{u}_i}{\bar{u}_i} \exp(-i\omega_r \tau), \quad (5)$$

238 where  $n$  is the acoustic-combustion interaction index,  $\tau$  the time delay be-  
 239 tween the velocity fluctuations in a reference point  $\hat{u}_i$  and the heat release  
 240 rate fluctuations  $\hat{q}$ . The minus sign derives by the definition of the n- $\tau$  model  
 241 in terms of fluctuations of equivalence ratio  $\hat{\phi}/\bar{\phi} = -\hat{u}/\bar{u}$  [47]. In order to ex-  
 242 amine only the phase shift induced by the flame and considering that always  
 243 time delays smaller than the period of the analysed mode are assumed only  
 244 the real part ( $\omega_r$ ) of the angular frequency  $\omega$  is considered in the flame model  
 245 of Eq. (5). The FTFs so modelled can be directly compared with the mea-  
 246 sured FTFs that are also defined in terms of the frequency of  $\omega_r$  of the forcing  
 247 signal used to measure the flame response [48].

### 248 3.2. The nonlinear flame models

249 Following Dowling [13], a theoretical nonlinear flame model is expressed  
 250 as the product of the linear flame transfer function ( $\mathcal{T}_L(\omega_r)$ ) shown in Eq. (5),  
 251 which depends only on frequency, by another function that depends only on  
 252 the amplitude of velocity fluctuations taken at the same reference point  $i$

253 defined in Eq. (5)<sup>1</sup>. This function is referred as *Nonlinear Flame Transfer*  
 254 *Function* NFTF( $|\hat{u}/\bar{u}|$ ) [24, 49] and introduce a saturation of the gain  $G$  of  
 255 the FTF with the increase of the amplitude of velocity fluctuations  $|\hat{u}/\bar{u}|$ .  
 256 Under these assumptions, the analytical frame describing function becomes

$$\mathcal{T}_{flame}^{NL}(\omega_r, |\hat{u}/\bar{u}|) = \mathcal{T}_L(\omega_r) \cdot \text{NFTF}(|\hat{u}/\bar{u}|). \quad (6)$$

257 The NFTF function derives directly from the nonlinearity introduced  
 258 into the flame model and it can be computed taking the first order of the  
 259 Fourier transform of the flame model formulated in the time domain (more  
 260 details can be found in the Appendix 1). Hereafter are reported the NFTF  
 261 functions for two flame models used in this study in which the heat release  
 262 rate fluctuations are related to the velocity fluctuations through a third-  
 263 order and a fifth-order polynomial law. In both cases, only the influence  
 264 of the odd-powered polynomial terms are examined because, although even-  
 265 powered polynomial terms are physically admissible, their contribution to  
 266 the acoustic energy integrates to zero over a cycle, as can be observed in  
 267 Appendix 1. The nonlinear flame model in which the third-powered term is  
 268 the highest order is

$$\frac{\dot{q}'(t)}{\bar{q}} = -n \left[ \mu_2 \left( \frac{u'(t-\tau)}{\bar{u}} \right)^3 + \mu_0 \frac{u'(t-\tau)}{\bar{u}} \right], \quad (7)$$

269 where the coefficient  $\mu_0$  is chosen equal to unity noting that for  $|\hat{u}/\bar{u}| \rightarrow 0$   
 270 the nonlinear flame model should tends to the linear model. The coefficient  
 271  $\mu_2$  is negative and its value is related to the effects of saturation of the flame

---

<sup>1</sup>In the remaining part of the article the subscript  $i$  will be omitted to improved the readability of equations.

272 response with large velocity fluctuations that are observed [44]. A parametric  
 273 system identification technique based on engine data can be used, as proposed  
 274 by Noiray *et al.* [35], in order to evaluate the third-order polynomial flame  
 275 model. In this study  $\mu_2=-2$ . The function NFTF for this model (algebraic  
 276 steps are shown in the Appendix 1) results

$$\text{NFTF} = \frac{3}{4}\mu_2|\hat{u}/\bar{u}|^2 + \mu_0. \quad (8)$$

277 The pattern of the NFTF function of Eq. (7) is shown in Fig. 3. Only  
 278 positive values of the amplitude  $|\hat{u}/\bar{u}|$  are considered to ensure the physical  
 279 meaning of the flame model. It is possible to observe that the NFTF man-  
 280 ifests a monotone decreasing pattern for increasing amplitudes until zero is  
 281 reached for  $|\hat{u}/\bar{u}|=0.81$ . The NFTF is assumed null also for higher values of  
 amplitude of velocity fluctuations.

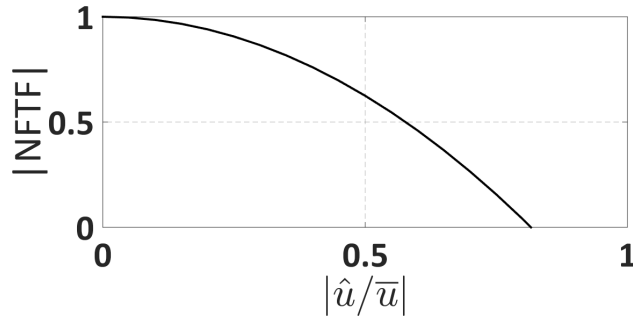


Figure 3: Pattern of the NFTF function for the third-order polynomial flame model of Eq. (7) with  $\mu_0=1$  and  $\mu_2=-2$ .

282

283 The nonlinear flame model in which the fifth-powered term is the highest  
 284 order is

$$\frac{\dot{q}'(t)}{\bar{q}} = -n \left[ \mu_4 \left( \frac{u'(t-\tau)}{\bar{u}} \right)^5 + \mu_2 \left( \frac{u'(t-\tau)}{\bar{u}} \right)^3 + \mu_0 \frac{u'(t-\tau)}{\bar{u}} \right], \quad (9)$$



285 where  $\mu_4$ ,  $\mu_2$  and  $\mu_0$  are coefficients equal to  $-5$ ,  $5$  and  $1$ , respectively. The  
 286 function NFTF for this model (see Appendix 1) is

$$\text{NFTF} = \frac{5}{8}\mu_4|\hat{u}/\bar{u}|^4 + \frac{3}{4}\mu_2|\hat{u}/\bar{u}|^2 + \mu_0. \quad (10)$$

287 The pattern of the NFTF function of Eq. (7) is shown in Fig. 4. Differently  
 288 from the previous case shown in Fig. 3 the function has an initial increase  
 289 reaching its maximum value, after which it decreases until zero is reached at  
 $|\hat{u}/\bar{u}|=1.19$ .

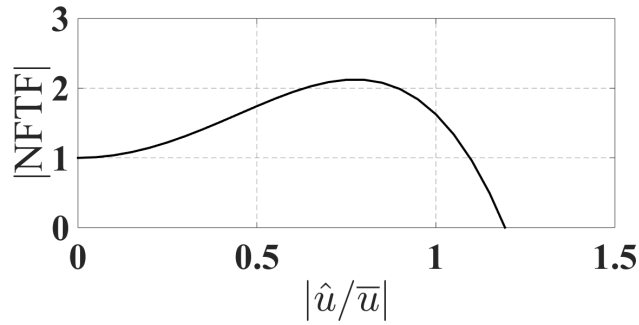


Figure 4: Patterns of the NFTF function for the fifth-order polynomial flame model of Eq. (9) with  $\mu_0=1$ ,  $\mu_2=5$  and  $\mu_4=-5$ .

290

### 291 3.3. Linear and weakly nonlinear stability analysis

The numerical analysis is carried out by using the finite element method (FEM) based the commercial software *Comsol Multiphysics*. This code solves the classical Helmholtz equation in which the heat release rate fluctuations are treated as pressure source. In order to include the damping, the second term of the Eq. (2) ( $-\lambda\zeta/\bar{c}\mathcal{L}\hat{p}$ ) is considered on the RHS of the equation

together with the heat release rate fluctuations

$$\left\{ \begin{array}{l} \frac{\lambda^2}{\bar{c}^2} \hat{p} - \bar{\rho} \nabla \cdot \left( \frac{1}{\bar{\rho}} \nabla \hat{p} \right) = -\frac{\gamma - 1}{\bar{c}^2} \lambda \hat{q} + \frac{\lambda \zeta}{\bar{c} \mathcal{L}} \hat{p} \end{array} \right. \quad (11)$$

$$\left\{ \begin{array}{l} \hat{q} = \bar{q} \frac{\hat{u}}{\bar{u}} \text{NFTF} e^{-i\omega_r \tau} \end{array} \right. \quad (12)$$

$$\left\{ \begin{array}{l} i\omega \hat{u} + \frac{1}{\bar{\rho}} \nabla \hat{p} = 0 \end{array} \right. \quad (13)$$

292 The finite element discretization of this set of equations along with the bound-  
 293 ary conditions results to the following eigenvalue problem [9]

$$[A] \mathbf{P} + \omega [B(\omega)] \mathbf{P} + \omega^2 [C] \mathbf{P} = [D(\omega)] \mathbf{P}, \quad (14)$$

294 where  $\mathbf{P}$  is the pressure eigenmodes vector, the matrices  $[A]$  and  $[C]$  contain  
 295 coefficients originating from the discretization of the Helmholtz equation,  
 296  $[B(\omega)]$  is the matrix of the boundary conditions and of the damping and  
 297  $[D(\omega)]$  represents source term due to the unsteady heat release rate. In case  
 298 of a linear stability analysis, i.e., assuming  $|\hat{u}/\bar{u}| \rightarrow 0$ , the NFTF equals unity  
 299 and Eq. (12) can be directly used to model the heat release rate fluctuations  
 300 in Eq. (11). However, with the introduction of the heat release the eigenvalue  
 301 problem of Eq. (14) becomes nonlinear and is solved with an iterative algo-  
 302 rithm. At the  $k^{th}$  iteration equation (14) is first reduced to a linear eigenvalue  
 303 problem around a specific frequency  $\Omega_k$

$$([A] + \Omega_k [B(\Omega_k)] - [D(\Omega_k)]) \mathbf{P} + \omega_k^2 [C] \mathbf{P} = 0, \quad (15)$$

304 where  $\Omega_k = \omega_{k-1}$  is the previous iteration result. The software uses the  
 305 *ARPACK* numerical routine for large-scale eigenvalue problems. This is  
 306 based on a variant of the Arnoldi algorithm, called the implicit restarted

307 Arnoldi method [50]. This procedure is iterated until the error defined by  
308  $\epsilon = |\omega_k - \Omega_k|$  is lower than a specific value, typically  $10^{-6}$ .

309 For finite value of velocity fluctuations, the NFTF of Eq. (12) depends  
310 on the value of  $|\hat{u}/\bar{u}|$ . As already shown in previous works [7, 29] the weakly  
311 nonlinear approach allows to couple a linear tool, i.e., the eigenvalue analysis,  
312 with a nonlinear function linearizing the nonlinear term. This is obtained  
313 performing the eigenvalue analysis assuming an initial guess for the value of  
314 velocity fluctuations  $|\hat{u}/\bar{u}|$  and reiterating this analysis increasing  $|\hat{u}/\bar{u}|$  until  
315 the limit cycle condition, i.e.,  $\alpha=0$  condition, is reached. For the calculation  
316 of the bifurcation diagrams, this numerical procedure is performed for each  
317 value of the acoustic-combustion interaction index  $n$ .

## 318 4. Results and discussion

319 The nonlinear behaviour of the flame modes of the third-order polynomial  
320 and fifth-order polynomial will be investigated. Two different configurations  
321 are examined: a longitudinal combustor with a single heat release zone and  
322 an annular combustor with multiple burners.

### 323 4.1. The longitudinal combustor

324 The first configuration analysed is a simple longitudinal combustor with  
325 a compact flame located in a narrow domain at around one quarter of the  
326 tube length, which is 3 m [10, 12]. Figure 5 shows the computational mesh  
327 and the location of the heat release is highlighted. The temperature increases  
328 from 300 K to 700 K across the combustion zone. An open condition,  $p'=0$ ,  
329 is assumed at the inlet section and outlet section of the domain.

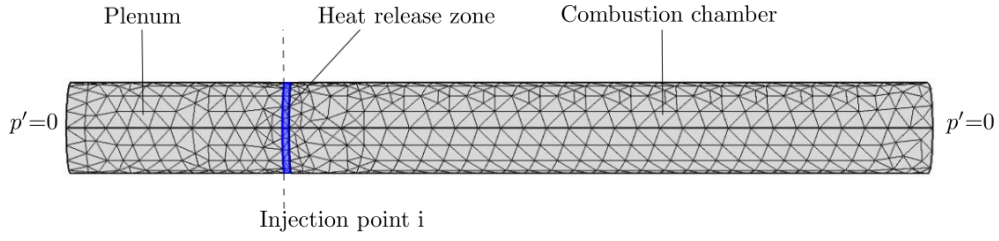


Figure 5: Computational mesh of the longitudinal combustor. The flame location is highlighted in blue.

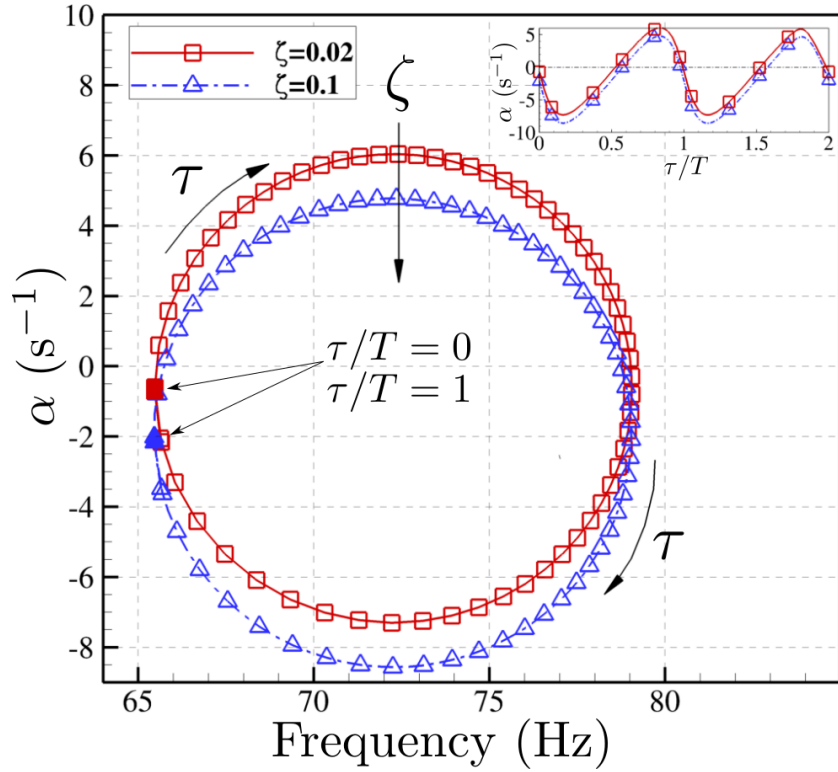


Figure 6: Frequency and growth rate ( $\alpha$ ) of the first eigenmode of the longitudinal combustor considering the flame model of Eq. (6) under the hypothesis of  $|\hat{u}/\bar{u}| \rightarrow 0$ .

330 At first, under the assumption of  $|\hat{u}/\bar{u}| \rightarrow 0$ , a linear stability analysis is  
 331 performed considering the linear flame transfer function expressed in Eq. (5).

332 Considering the compactness of the flame, the time delay  $\tau$  is assumed con-  
 333 stant in the flame model. This analysis is useful to have a better comprehen-  
 334 sion of the influence on the system of the time delay and of the damping. In  
 335 Fig. 6, the growth rate ( $\alpha$ ) is plotted against the frequency for the first axial  
 336 mode of the system for different values of time delay  $\tau$ , which is expressed  
 337 normalized against the period of the mode  $T$ . The time delay  $\tau$  is varied in  
 338 order to keep  $\tau/T$  from 0 to 1. The patterns are tracked for two values of  
 339 the damping coefficient:  $\zeta$  equal to 0.02 and 0.1. The acoustic-combustion  
 340 interaction index  $n$  is kept equal to unity for this analysis. Figure 6 shows  
 341 that frequency and growth rate decrease or increase depending on the value  
 342 of the time delay assumed. Circular patterns like the ones found in [7] are  
 343 found. This result is due to the chosen FTF where only the real part of  
 344 the frequency is considered. Increasing the damping coefficient results in  
 345 a vertical shift of the patterns towards more stable condition, i.e., growth  
 346 rates decrease. The frequencies remain constant (frequency shifts are under  
 347 1 Hz). This is justified remembering that the frequency variation depends on  
 348 the ratio between  $\alpha/\omega_r$ . If  $\alpha/\omega_r \ll 1$  the complex frequency  $\omega \sim \omega_r$  [51]. It  
 349 should be notice that for the analysed condition this ratio is always far below  
 350 the unity, e.g., in the condition where the absolute value of  $\alpha$  is maximum  
 351  $\alpha/frequency \sim 8/75 \sim 0.07$ .

352 When a finite level of velocity fluctuations is considered in the model, a  
 353 harmonic base weakly nonlinear stability analysis is performed and the bifur-  
 354 cation diagrams are mapped considering the acoustic-combustion interaction  
 355 index  $n$  as the control parameter. Figure 8 shows the bifurcation diagram  
 356 when the nonlinear flame model of Eq. (8), in which the third-powered term

357 is the highest order, is introduced. A supercritical bifurcation is observed.  
 358 The influence of the damping coefficient  $\zeta$  and the time delay  $\tau$  is examined  
 359 and results are reported in Fig. 8a and Fig. 8b, respectively. In both dia-  
 360 grams, the rectangular marks indicate the position of the Hopf bifurcation  
 361 point. For a fixed value of time delay equal to 11 ms ( $\tau/T=0.78$ ), the damp-  
 362 ing coefficient  $\zeta$  is varied from 0 to 0.3. The black dashed line in Fig. 8a  
 363 corresponds to the zero-damping condition, i.e.,  $\zeta=0$ . It is possible to ob-  
 364 serve that the system is unstable for any value of the control parameter  $n$   
 365 except for the condition with  $n=0$ . Furthermore, the amplitude of the limit  
 366 cycle is constant and corresponds to the value that saturates the gain of the  
 367 nonlinear flame model (the NFTF function) and nullifies the heat release rate  
 368 fluctuations, as it is possible to observe in Fig. 8. For the specific case, this  
 369 value of  $|\hat{u}/\bar{u}|$  is equal to 0.81. When considering  $\zeta$  non-zero, the position of  
 370 the Hopf point moves towards higher values of the control parameter  $n$  as  
 371 the damping level increases. For higher value of the acoustic-combustion in-  
 372 teraction index, the increase of the energy dissipation rate causes a reduction  
 373 of the amplitude of oscillations. However, due to the nonlinear saturation of  
 374 the heat release rate, regardless the damping level, the amplitude  $|\hat{u}/\bar{u}|$  tends  
 375 asymptotically to the value, which saturates the heat release rate. In Fig. 8b  
 376 for a fixed value of  $\zeta=0.1$  the time delay is varied from 8 ms to 13 ms. Starting  
 377 from the condition in which the maximum amplitude of velocity fluctuation  
 378 is registered, i.e.,  $\tau=11$  ms, which corresponds to the more unstable condi-  
 379 tion in the linear stability analysis, an increase or decrease of the time delay  
 380 produces a shift of the transition point at higher levels of the coefficient  $n$   
 381 and a decrease of the amplitude of velocity fluctuation for a given value of  $n$ .

382 Table 1 summarize the values of the frequencies in the Hopf point ( $f_{Hopf}$ ).  
 383 As shown in Fig. 6 the damping has small influence in the frequency, which  
 384 varies only with the time delay  $\tau$ . In particular, starting from the condition  
 385 with the time delay equal to 8 ms, a reduction of the frequency is registered  
 386 increasing  $\tau$ . Figure 7 shows the wave shape of the resonant mode in the  
 387 condition with  $\tau=11$  ms.

Table 1: Frequencies at the Hopf point ( $f_{Hopf}$ ) for the nonlinear flame model of Eq. (7) for different time delays  $\tau$ . Time delays are expressed in milliseconds. Frequencies in Hertz (Hz).

	$\tau=8$	$\tau=9$	$\tau=10$	$\tau=11$	$\tau=12$	$\tau=13$
$f_{Hopf}$	74.8	73.6	72.7	71.5	69.5	66

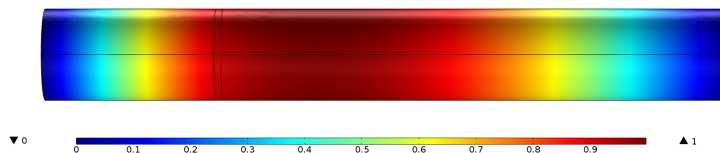
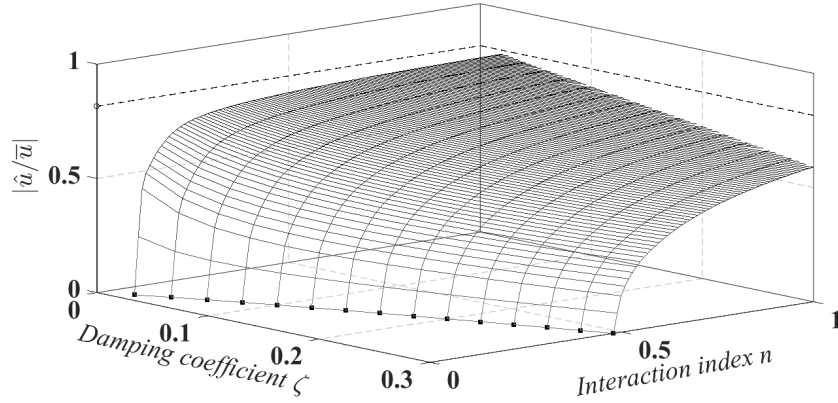
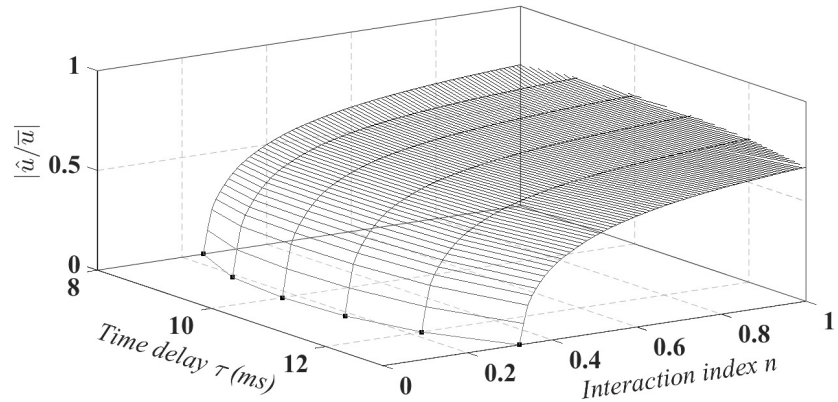


Figure 7: Normalized absolute pressure of the first longitudinal mode of the combustion chamber considering a time delay equal to 11 ms.

388 A different behaviour is registered when the nonlinear flame model of  
 389 Eq. 9, in which the fifth-power term is the highest order, is introduced into  
 390 the model. In this case, the system undergoes a subcritical bifurcation as  
 391 is shown in Fig. 9. The continuous black lines indicate the stable branch of  
 392 the diagram, while the unstable branch is reported with dashed lines. Both  
 393 the Hopf bifurcation point and the fold bifurcation point are indicated with



(a)



(b)

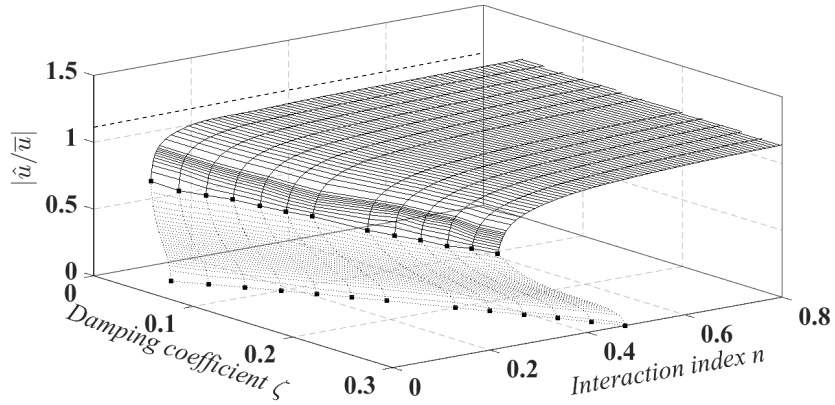
Figure 8: Bifurcation surfaces when the nonlinear flame model of Eq. (7) is considered. (a) influence of the damping coefficient  $\zeta$  with a time delay  $\tau=11$  ms; (b) influence of the time delay  $\tau$  with  $\zeta=0.1$ .

394 rectangular marks. Starting from the Hopf bifurcation point, the proposed  
 395 numerical technique is able to converge also in the unstable zone of the  
 396 diagram. Also for this case a sensitivity analysis to the damping coefficient  
 397  $\zeta$  and the time delay  $\tau$  is performed. Similar to the previous case, in Fig. 9a  
 398 for a fixed value of time delay of 11 ms, the damping coefficient  $\zeta$  is varied

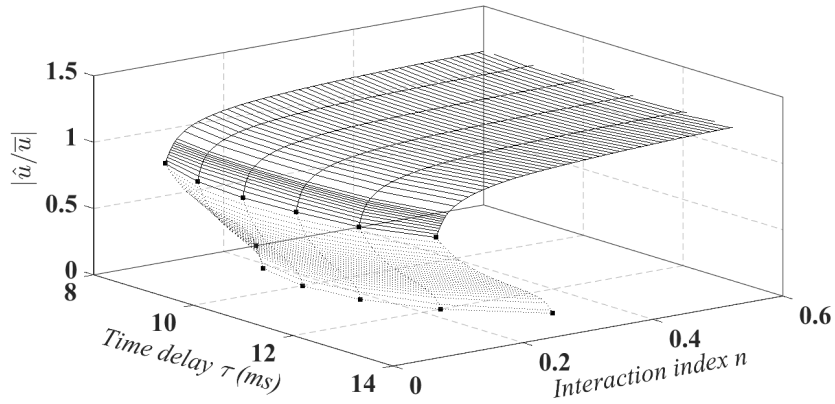


399 from zero to 0.3. If no damping is considered, the system results always  
 400 unstable except for the case with  $n=0$  (dashed line in Fig. 9a). Differently  
 401 from the previous flame model, the saturation of the NFTF function occurs  
 402 at a higher amplitude value equals to 1.19 as it is possible to observe from  
 403 Fig. 4. Increasing the damping level results in a shift towards higher values  
 404 of the control parameter  $n$  of both the Hopf bifurcation point and the fold  
 405 point. On the contrary, the velocity amplitude  $|\hat{u}/\bar{u}|$  corresponding to the  
 406 fold bifurcation point is not influenced by the level of the damping. This  
 407 behaviour is typical of systems that manifest a subcritical bifurcation as  
 408 shown in Subramanian *et al.* [5] where similar results are found for a different  
 409 flame model and with a different methodology. As noticed with the first  
 410 nonlinear flame model, the amplitude of the stable limit cycle solution tends  
 411 to be the same for all the cases at high values of  $n$ . In Fig. 9b for a fixed  
 412 value of  $\zeta=0.1$  the time delay is varied from 8 ms to 13 ms. Again, starting  
 413 from the more unstable condition at  $\tau=11$  ms, a variation of the time delay  
 414 induces a shift of the Hopf point and the fold point towards higher level of  
 415  $n$ . The amplitude of the fold bifurcations remains constant.

416 To verify these results, the two flame models of Eq. (7) and Eq. (9) are  
 417 considered in the Low-order code “OSCILOS” [52]. Only the bifurcations  
 418 diagrams with  $\zeta=0.1$  and  $\tau=11$  ms are computed in the analytic framework  
 419 assuming similar for the other configurations. Since in the low-order code the  
 420 acoustic waves are modelled as 1-D plane waves without the possibility to  
 421 add the damping term of Eq.(11), the eigenvalue procedure is reiterated for  
 422 different amplitude levels starting from  $|\hat{u}/\bar{u}|=0$  and incrementing this value  
 423 until a limit cycle condition which is reached when  $\alpha=\delta$  with the damping



(a)



(b)

Figure 9: Bifurcation surfaces when the nonlinear flame model of Eq. (9) is considered. (a) influence of the damping coefficient  $\zeta$  with time delay  $\tau=11$  ms; (b) influence of the time delay  $\tau$  with a damping coefficient  $\zeta=0.1$ .

424 rate  $\delta=2.22\text{ s}^{-1}$  computed by means of simulations in the Helmholtz solver  
 425 under “passive flame” conditions, i.e., considering only the steady combus-  
 426 tion process with  $\hat{q}=0$  in Eq. (11). Figure 10 shows that there is a perfect  
 427 overlap between the analytical results and the results of the Helmholtz solver  
 428 calculations, for the supercritical and the subcritical case.

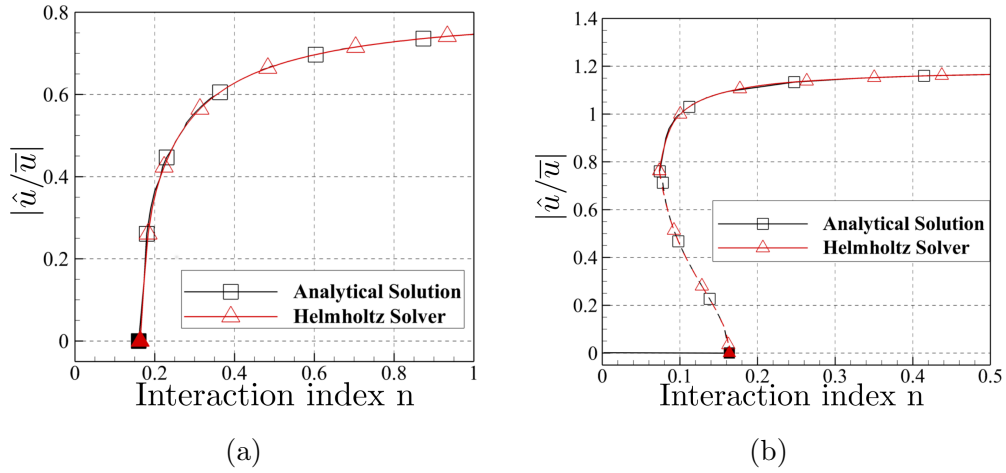


Figure 10: Comparison between the supercritical (a) and subcritical (b) bifurcation diagrams assuming  $\tau=11$  ms and  $\zeta=0.1$  computed with the Helmholtz solver (red line) and the analytical low-order code “OSCILOS” (black line).

#### 4.2. Annular Combustion Chamber

The Helmholtz solver approach allows the nonlinear analysis on complex geometries that can be also characterized by the presence of multiple flames. In this section, the nonlinear behaviour of an annular combustor characterized by a plenum and an annular combustion chamber connected by a ring of twelve straight ducts (representing the burners) is analysed. The geometrical configuration is similar to the one introduced by Pankiewitz and Sattelmayer [39]. The mean diameter is 0.437 m, the external diameter of the plenum is 0.540 m and of the combustion chamber is 0.480 m. The length of the plenum is 0.200 m and of the combustion chamber is 0.300 m. Each burner has a diameter of 0.026 m and a length of 0.030 m. Temperature in the combustion chamber is 2.89 times the temperature on the plenum. Flame is assumed to be concentrated in a narrow zone at the entrance of the combus-

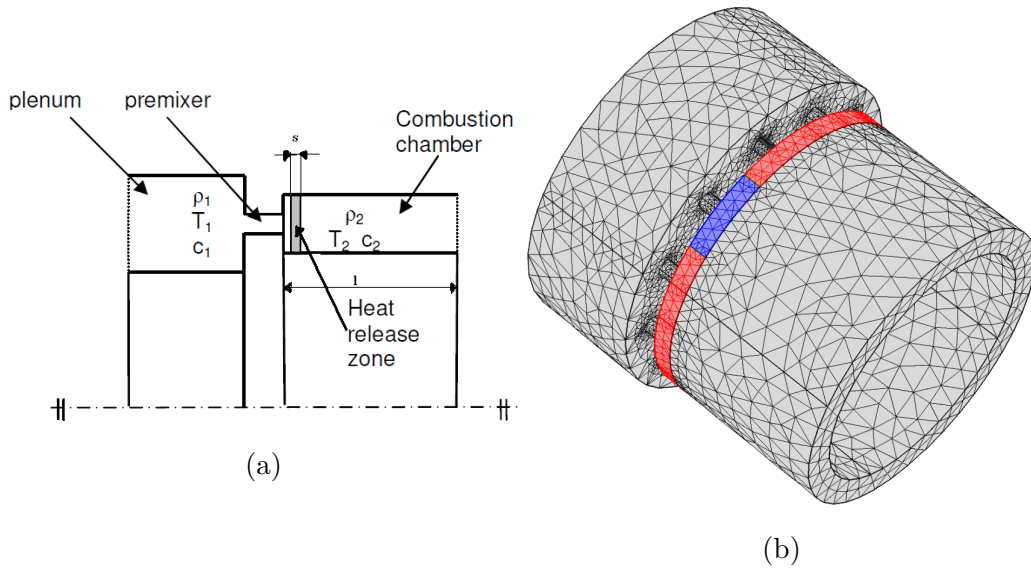


Figure 11: (a) Sketch of the annular combustion chamber. (b) Computational grid and flame zone highlighted in red. One of the twelve sectors, in which the flame zone is divided, is highlighted in blue.

442 tion chamber, as shown in Fig. 11, it is composed of twelve equal parts, one  
 443 corresponding to each burner and, differently from what is done with other  
 444 approaches [34, 35, 36] in each of them the flame model is defined. In so  
 445 doing the heat release rate fluctuations are coupled to the velocity fluctua-  
 446 tions of the corresponding burner, following the ISAAC (Independence Sector  
 447 Assumption in Annular Combustors) assumption, introduced by Sensiau *et*  
 448 *al.* [53]. This assumption states that *the heat release rate fluctuations in a*  
 449 *given sector [of the combustion chamber] are only driven by the fluctuating*  
 450 *mass flow rates due to the velocity perturbations through its own swirler.* Fur-  
 451 thermore, following Wolf *et al.* [54] only the axial component of the velocity  
 452 fluctuations is assumed to influence the flame dynamics. In the model, the

453 reference point for the velocity fluctuations is considered in the middle of the  
454 burner, where the injection of the premixed mixture is usually located. In  
455 this work all burner are assumed to undergo the same velocity fluctuations  
456 level feature that is proper of a spinning mode [36]. Annular combustors can  
457 feature also standing and mixed azimuthal instabilities [14, 35] in which the  
458 burners operate with different amplitude of velocity fluctuations depending  
459 on the relative position with respect to the nodal line. Once the distribution  
460 of the velocity fluctuations is accounted, the numerical procedure to track the  
461 limit cycle conditions is identical to the one proposed in this article. In the  
462 analysed configuration, closed-end inlet and outlet are assumed as boundary  
463 conditions ( $u'=0$ ). Losses due to viscous and thermal boundary layers are  
464 considered in the entire computational domain. In the plenum and in the  
465 combustion chamber a characteristic length ( $\mathcal{L}$ ) of 0.212 m and 0.137 m, re-  
spectively, is used in the damping term of Eq. (11). Mean flow is neglected

Table 2: Frequencies of the first four modes of the annular combustor. Subscript “p” stands for plenum and “cc” for the combustion chamber

Mode Shape	(1,0,0)	(0,1 <sub>p</sub> ,0)	(0,1 <sub>cc</sub> ,0)	(0,2,0)
Frequency Hz	309.4	446.5	734.8	839.3

466  
467 also in this case. Table 2 shows the first four modes of the system without  
468 heat release rate fluctuations. Eigenmodes are denoted with the nomencla-  
469 ture  $(l, m, n)$ , where  $l$ ,  $m$  and  $n$  are, respectively, the orders of the pure axial,  
470 circumferential and radial modes.

471 For such configuration the most interesting mode is the first azimuthal

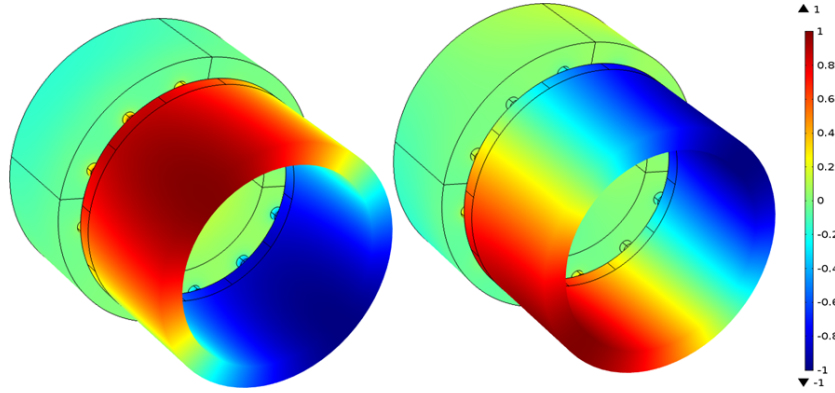


Figure 12: Wave shapes shifted of  $\pi/2$  of the first azimuthal degenerate mode of the combustion chamber (mode (1,1,0) in Tab. 2) reported in terms of normalized acoustic pressure.

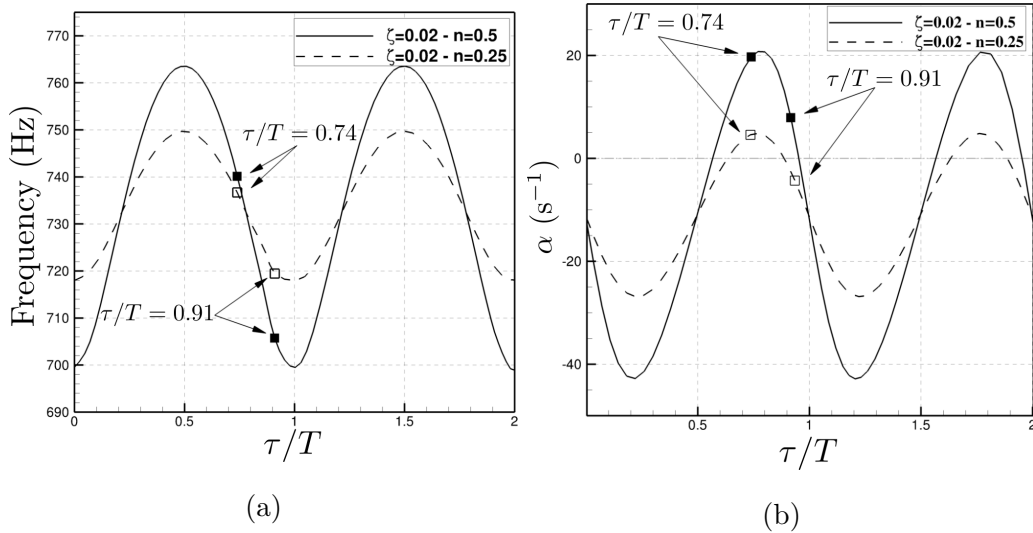


Figure 13: Frequency (a) and growth rate ( $\alpha$ ) (b) of the azimuthal mode in the combustion chamber for  $|\hat{u}/\bar{u}| \rightarrow 0$ .

472 mode in the combustion chamber (mode (0,1<sub>cc</sub>,0) in Tab. 2), since it is the  
 473 most prone mode to experience instabilities in practical machines [40]. Fig-  
 474 ure 13 shows the results frequencies and growth rates of the linear stability

475 analysis ( $|\hat{u}/\bar{u}| \rightarrow 0$ ) considering a damping coefficient  $\zeta=0.02$  and two differ-  
 476 ent values for the combustion-acoustic interaction index  $n$ . The time delay  
 477 is varied from  $\tau/T=0$  to  $\tau/T=2$ . In order to analyse the results of Fig. 13,  
 478 following Lieuwen *et al.* [55], if the inlet section of the injector connected  
 479 to a large plenum can be approximated as a pressure node, in the linear  
 480 case without damping the regions of instability is predicted in bands where  
 481  $C_k - 1/4 < \tau/T < C_k + 1/4$ , being  $C_k=k-1/4$  ( $k=1,2,\dots$ ). In Fig. 13, due  
 482 to the presence of the damping, results are different. With  $n=0.25$ , the  
 483 mode is unstable only for  $0.65 < \tau/T < 0.9$  and  $1.65 < \tau/T < 1.9$  (dashed  
 484 lines in Fig. 13). Increasing the interaction index results a shift towards  
 485 more unstable conditions. Assuming an interaction index  $n=0.5$  the regions  
 486 of instabilities predicted by Lieuwen *et al.* [55] are obtained (solid lines in  
 487 Fig. 13). So, in this configuration, the system passes from stable to unsta-  
 488 ble conditions for  $\tau/T = k - 1/2$  ( $k=1,2,\dots$ ), while from unstable to stable  
 489 conditions for  $\tau/T=k$  ( $k =1,2,\dots$ ). It means that each of these conditions  
 490 can be identified as bifurcation points in the nonlinear case. With the as-  
 491 sumption of considering the same amplitude of velocity fluctuations for each  
 492 burner the circumferential symmetry of the system is conserved. For each  
 493 level of velocity fluctuations  $|\hat{u}/\bar{u}|$ , the eigenvalue analysis for the first az-  
 494 imuthal mode is degenerate. Combining the two mode structures shifted of  
 495  $\pi/2$  shown in Fig. 12, a spinning mode is obtained [38]. Two conditions are  
 496 taken into account:  $\tau/T=0.74$  and  $\tau/T=0.91$ . The bifurcation diagrams for  
 497 these two cases are tracked and shown in Fig. 14 considering both the flame  
 498 models of Eq. (7) and Eq. (9). Again, a supercritical and a subcritical bifur-  
 499 cation occurs. The limit cycle for the two configurations occurs at different

500 frequency which remain constant increasing of the control parameter: in the  
 501 case of  $\tau/T=0.74$ , it occurs at 735.9 Hz; in the case of  $\tau/T=0.91$ , it occurs  
 502 at 713.6 Hz. The influence of the time delay is again on the position of the  
 503 Hopf point and fold point: a shift towards high value of  $n$  is observed with a  
 504 higher  $\tau/T$  is considered. In the subcritical bifurcation case, as for the longi-  
 505 tudinal configuration, the amplitude of the fold point remains constant. Also  
 506 in this configuration, the influence of the time delay decreases increasing the  
 507 acoustic-combustion interaction index  $n$ . Both curves tends asymptotically  
 508 to the value, which saturates the NFTF.

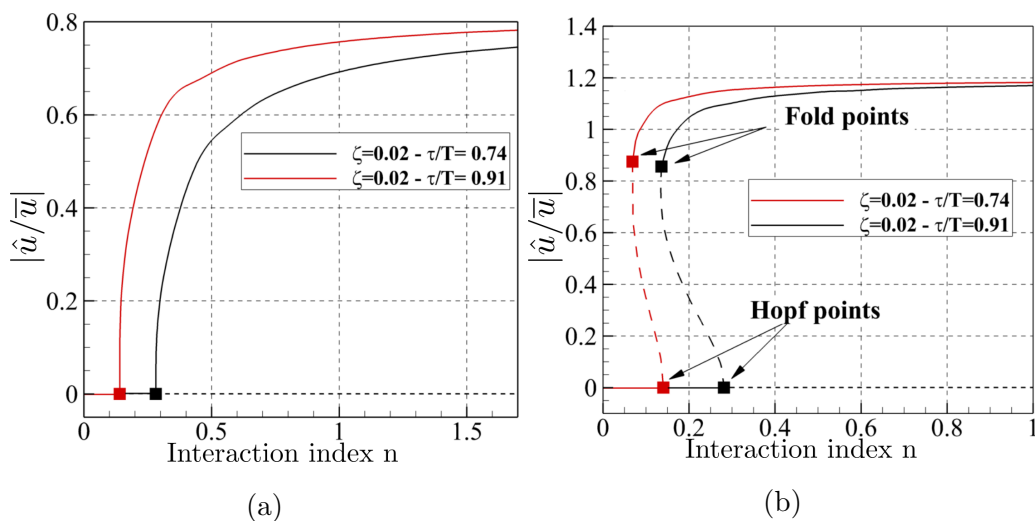


Figure 14: Bifurcation diagrams of the first azimuthal mode in the combustion chamber of the annular combustion chamber in Fig. 11 with: (a) the nonlinear flame model of Eq. (9); (b) the nonlinear flame model of Eq. (7).



## 509 5. Conclusions

510 A numerical approach based on the use of the Helmholtz solver in order  
511 to study the limit cycles of longitudinal and azimuthal modes is presented  
512 in this article. The numerical procedure has been implemented in a FEM  
513 code able to treat any kind of three-dimensional geometries, with single and  
514 multiple burners. At first on a simple longitudinal combustor has been ex-  
515 amined considering two nonlinear flame models consisting of a time delayed  
516 third-order polynomial and fifth-order polynomial saturation law. For this  
517 case, the bifurcation diagrams have been tracked evaluating the amplitude of  
518 the limit cycles at assuming the acoustic-combustion interaction index  $n$  as  
519 control variable. Two kinds of bifurcation have been found, depending on the  
520 nonlinear flame model. The third-order polynomial law features a supercrit-  
521 ical bifurcation, whereas, the fifth-order polynomial nonlinear flame model  
522 features a subcritical bifurcation. The numerical approaches have been val-  
523 idating comparing the results against bifurcation diagrams obtained in the  
524 same configuration with an analytical tool. In a second step, an annular  
525 combustor equipped with twelve independent burners have been considered  
526 proving the ability of the proposed numerical technique to study the limit  
527 cycles occurring also in multiple flames configurations. The influence on the  
528 bifurcation of the time delay of the flame model and of the amount of damp-  
529 ing considered in the system have been, subsequently, investigated in both  
530 configurations. As expected, increasing the damping coefficient, the ampli-  
531 tude of  $|\hat{u}/\bar{u}|$  at limit cycles decreases. The time delay mainly influences the  
532 position of the Hopf bifurcation point and, in case of a subcritical bifurca-  
533 tion, of the fold point. On the contrary, the amplitude of the limit cycle at

534 the fold point are not influenced by variations of the time delay. In both bi-  
535 furcation behaviours at high values of the control parameter, the influence of  
536 the time delay and of the damping coefficient is low. The amplitude of limit  
537 cycles tends asymptotically to the value which nullifies the heat release rate  
538 fluctuations due to the saturation process induced by the nonlinear terms.  
539 The proposed approach proves to be able to treat nonlinear problems with  
540 simple configurations and, differently from other approaches described in the  
541 literature, more complex multi-burner configurations can be analysed mak-  
542 ing the described numerical approach to be also employed in an industrial  
543 environment. Numerical and experimental data can be introduced into the  
544 simulation model, performing parametric analyses which can be helpful both  
545 in the design and in the check stage of a burner.

## 546 **Appendix 1: Nonlinear flame model derivation**

547 Let consider the nonlinear flame model in Eq. (7) where the third-powered  
548 term is the highest order. The flame model is converted into the frequency  
549 domain assuming the flame response to a harmonic input

$$u'(t) = Re(\hat{u}e^{i\omega t}) = |\hat{u}| \cos(\omega t). \quad (16)$$

550 For finite disturbances, the flame model  $\dot{q}'(t)$  may not be pure harmonic but  
551 is still periodic and hence it can be described by a Fourier series:

$$\dot{q}'(t) = Re\left(\sum_{m=0}^{\infty} \hat{q}^m e^{im\omega t}\right), \quad (17)$$

552 where  $m$  is the order of the harmonics. Let now consider the first harmonic  
553  $\hat{q}^{(1)}$ . The nonlinear flame transfer function NFTF to be derived is a function

554 of frequency and amplitude  $|\hat{u}/\bar{u}|$ . The first Fourier coefficient is written as

$$\hat{q}^{(1)} = \frac{\omega}{\pi} \int_0^{2\pi/\omega} \dot{q}' e^{i\omega t} dt. \quad (18)$$

555 Introducing Eq. (16), Eq. (17) and the nonlinear flame model in Eq. (7),  
 556 and considering the property of the Fourier transform that  $F(u'(t - \tau)) =$   
 557  $F(u'(t))e^{-i\omega\tau}$  it is shown that

$$\begin{aligned} \hat{q}^{(1)} = & \frac{\omega}{\pi} \int_0^{2\pi/\omega} -n\bar{q}e^{-i\omega\tau} \left( \mu_2 \left| \frac{\hat{u}}{\bar{u}} \right|^2 \cos^2(\omega t) + \mu_0 \right) \left| \frac{\hat{u}}{\bar{u}} \right| \cos(\omega t) \left( \cos(\omega t) + \right. \\ & \left. + i \sin(\omega t) \right) dt = -n\bar{q} \left| \frac{\hat{u}}{\bar{u}} \right| e^{-i\omega\tau} \left( \frac{\omega}{\pi} \int_0^{2\pi/\omega} \mu_2 \cos^4(\omega t) \left| \frac{\hat{u}}{\bar{u}} \right|^2 dt + \right. \\ & \left. + \frac{\omega}{\pi} \int_0^{2\pi/\omega} \mu_0 \cos^2(\omega t) dt \right), \end{aligned} \quad (19)$$

558 where the imaginary term disappears because the integral from 0 to  $2\pi$  of  
 559 the product of cosine and sine is null. Additionally, it can be observed that  
 560 even-powered polynomial terms are not mathematically admissible, because  
 561 the cosine function is an even function and so the integral of its even-powered  
 562 terms between 0 and  $2\pi$  is null. Solving the integrals in Eq. (19) and consid-  
 563 ering that  $\hat{q}^L = -n\bar{q}|\hat{u}/\bar{u}|e^{-i\omega\tau}$

$$\hat{q}^{(1)} = \hat{q}^L \left( \frac{3}{4} \mu_2 \left| \frac{\hat{u}}{\bar{u}} \right|^2 + \mu_0 \right), \quad (20)$$

564 which is the nonlinear flame model  $\mathcal{T}_{flame}^{NL}(\omega, |\hat{u}/\bar{u}|)$  of Eq. (6). Hence the  
 565 function NFTF shown in Eq. (8) is obtained.

566 For the nonlinear flame model in Eq. (9) where the fifth-powered term  
 567 is the highest order, considering the same assumption made for the first  
 568 nonlinear flame model, the first Fourier coefficient for the second nonlinear

569 flame model is written as

$$\begin{aligned}
\hat{q}^{(1)} &= \frac{\omega}{\pi} \int_0^{2\pi/\omega} -n\bar{q}e^{-i\omega\tau} \left( \mu_4 \left| \frac{\hat{u}}{\bar{u}} \right|^4 \cos^4(\omega t) + \mu_2 \left| \frac{\hat{u}}{\bar{u}} \right|^2 \cos^2(\omega t) + \mu_0 \right) \\
&\quad \left| \frac{\hat{u}}{\bar{u}} \right| \cos(\omega t) \left( \cos(\omega t) + i \sin(\omega t) \right) dt = -n\bar{q} \left| \frac{\hat{u}}{\bar{u}} \right| e^{-i\omega\tau} \left( \frac{\omega}{\pi} \int_0^{2\pi/\omega} \mu_4 \right. \\
&\quad \left. \cos^6(\omega t) \left| \frac{\hat{u}}{\bar{u}} \right|^4 dt + \frac{\omega}{\pi} \int_0^{2\pi/\omega} \mu_2 \cos^4(\omega t) \left| \frac{\hat{u}}{\bar{u}} \right|^2 dt + \frac{\omega}{\pi} \int_0^{2\pi/\omega} \mu_0 \cos^2(\omega t) dt \right),
\end{aligned} \tag{21}$$

570 where the imaginary term disappears because the integral from 0 to  $2\pi$  of the  
571 product of cosine and sine is null. Again, solving the integrals and considering  
572 that  $\hat{q}^L = -n\bar{q}|\hat{u}/\bar{u}|e^{-i\omega\tau}$

$$\hat{q}^{(1)} = \hat{q}^L \left( \frac{5}{8}\mu_4 \left| \frac{\hat{u}}{\bar{u}} \right|^4 + \frac{3}{4}\mu_2 \left| \frac{\hat{u}}{\bar{u}} \right|^2 + \mu_0 \right), \tag{22}$$

573 which is the (nonlinear) flame transfer function  $\mathcal{T}_{flame}^{NL}(\omega, |\hat{u}/\bar{u}|)$  of Eq .(6).

574 Hence the function NFTF shown in Eq. (8) is obtained.

## 575 References

- 576 [1] Fichera, A., Losenno, C., and Pagano, A., 2001. “Experimental analysis  
577 of thermo-acoustic combustion instability”. *Applied Energy*, **70**(2),  
578 pp. 179–191.
- 579 [2] Lieuwen, T. C., and Yang, V., 2005. “Combustion instabilities in gas  
580 turbine engines(operational experience, fundamental mechanisms and  
581 modeling)”. *Progress in astronautics and aeronautics*.
- 582 [3] Fichera, A., and Pagano, A., 2006. “Application of neural dynamic  
583 optimization to combustion-instability control”. *Applied energy*, **83**(3),  
584 pp. 253–264.

- 585 [4] Zhao, D., and Li, L., 2015. “Effect of choked outlet on transient energy  
586 growth analysis of a thermoacoustic system”. *Applied Energy*, **160**,  
587 pp. 502 – 510.
- 588 [5] Subramanian, P., Sujith, R., and Wahi, P., 2013. “Subcritical bifurcation  
589 and bistability in thermoacoustic systems”. *Journal of Fluid Mechanics*,  
590 **715**, pp. 210–238.
- 591 [6] Juniper, M., 2012. “Triggering in thermoacoustics”. *International Jour-  
592 nal of Spray and Combustion Dynamics*, **4**(3), pp. 217–238.
- 593 [7] Silva, C. F., Nicoud, F., Schuller, T., Durox, D., and Candel, S., 2013.  
594 “Combining a helmholtz solver with the flame describing function to  
595 assess combustion instability in a premixed swirled combustor”. *Com-  
596 bustion and Flame*, **160**(9), September, pp. 1743–1754.
- 597 [8] Zhang, Z., Zhao, D., Dobriyal, R., Zheng, Y., and Yang, W., 2015.  
598 “Theoretical and experimental investigation of thermoacoustics transfer  
599 function”. *Applied Energy*, **154**, pp. 131–142.
- 600 [9] Nicoud, F., Benoit, L., Sensiau, C., and Poinsot, T., 2007. “Acoustic  
601 modes in combustors with complex impedances and multidimensional  
602 active flames”. *AIAA journal*, **45**(2), pp. 426–441.
- 603 [10] Camporeale, S., Fortunato, B., and Campa, G., 2011. “A finite element  
604 method for three-dimensional analysis of thermoacoustic combustion in-  
605 stability”. *Journal of Engineering for Gas Turbine and Power*, **133**(1),  
606 p. 011506.

- 607 [11] Zhao, D., Li, S., Yang, W., and Zhang, Z., 2015. “Numerical investiga-  
608 tion of the effect of distributed heat sources on heat-to-sound conversion  
609 in a t-shaped thermoacoustic system”. *Applied Energy*, **144**, pp. 204–  
610 213.
- 611 [12] Dowling, A., and Stow, S., 2003. “Acoustic analysis of gas turbine  
612 combustors”. *Journal of Propulsion and Power*, **19**(5), pp. 751–765.
- 613 [13] Dowling, A., 1997. “Nonlinear self-excited oscillations of a ducted  
614 flame”. *Journal of Fluid Mechanics*, **346**, pp. 271–290.
- 615 [14] Bauerheim, M., Nicoud, F., and Poinsot, T., 2016. “Progress in ana-  
616 lytical methods to predict and control azimuthal combustion instability  
617 modes in annular chambers”. *Physics of Fluids (1994-present)*, **28**(2),  
618 p. 021303.
- 619 [15] Culick, F., 2006. *Unsteady Motions in Combustion Chambers for Propul-*  
620 *sion Systems*. AGARD, AG-AVT-039.
- 621 [16] Ananthkrishnan, N., Deo, S., and Culick, F., 2005. “Reduced-order  
622 modeling and dynamics of nonlinear acoustic waves in a combustion  
623 chamber”. *Combustion Science and Technology*, **177**, pp. 1–27.
- 624 [17] Strogatz, S., 2001. *Nonlinear Dynamics and Chaos*. Westview Press.
- 625 [18] Moeck, J., Bothien, M., Schimek, S., Lacarelle, A., and Paschereit, C.,  
626 2008. “Subcritical thermoacoustic instabilities in a premixed combus-  
627 tor”. *14th AIAA/CEAS Aeroacoustics Conference*, 2946.

- 628 [19] Jahnke, C., and Culick, F., 1994. “Application of dynamical systems  
629 theory to nonlinear combustion instabilities”. *Journal of Propulsion  
630 and Power*, **10**, pp. 508–517.
- 631 [20] Burnley, V., 1996. “Nonlinear Combustion Instabilities and Stochastic  
632 Sources”. PhD Dissertation, California Inst. of Technology, Pasadena,  
633 USA.
- 634 [21] Juniper, M., 2011. “Triggering in the horizontal rijke tube: Non-  
635 normality, transient growth and bypass transition”. *Journal of Fluid  
636 Mechanics*, **667**, pp. 272–308.
- 637 [22] Subramanian, P., Mariappan, S., Sujith, R., and Wahi, P., 2010. “Bifur-  
638 cation analysis of thermoacoustic instability in a horizontal rijke tube”.  
639 *Int. Journal of Spray and Combustion Dynamics*, **2**(4), pp. 325–356.
- 640 [23] Engelborghs, K., Luzyanina, T., and Roose, D., 2002. “Numerical bifur-  
641 cation analysis of delay differential equations using dde-biftool”. *ACM  
642 Transactions on Mathematical Software*, **28**, pp. 1–21.
- 643 [24] Campa, G., and Juniper, M., 2012. “Obtaining bifurcation diagrams  
644 with a thermoacoustic network model”. *ASME paper, GT2012-68241*.
- 645 [25] Dowling, A., 1999. “A kinematic model of a ducted flame”. *Journal of  
646 Fluid Mechanics*, **394**, pp. 51–72.
- 647 [26] Noiray, N., Durox, D., Schuller, T., and Candel, S., 2009. “A method for  
648 estimating the noise level of unstable combustion based on the flame de-  
649 scribing function”. *International Journal of Aeroacoustics*, **8**, pp. 157–  
650 176.

- 651 [27] Boudy, F., Durox, D., Schuller, T., Jomaas, G., and Candel, S., 2011.  
652 “Describing function analysis of limit cycles in a multiple flame com-  
653 bustor”. *Journal of Engineering for Gas Turbine and Power*, **133**(6),  
654 p. 061502.
- 655 [28] Boudy, F., Durox, D., Schuller, T., and Candel, S., 2011. “Nonlinear  
656 mode triggering in a multiple flame combustor”. *Proceedings of the  
657 Combustion Institute*, **33**(1), pp. 1121–1128.
- 658 [29] Palies, P., Durox, D., Schuller, T., and Candel, S., 2011. “Nonlinear  
659 combustion instability analysis based on the flame describing function  
660 applied to turbulent premixed swirling flames”. *Combustion and Flame*,  
661 **158**(10), pp. 1980–1991.
- 662 [30] Illingworth, S., Waugh, I., and Juniper, M., 2013. “Finding thermo-  
663 acoustic limit cycles for a ducted burke-schumann flame”. *Proceedings of  
664 the Combustion Institute*, **34**(1), pp. 911–920.
- 665 [31] Kabiraj, L., Sujith, R., and Wahi, P., 2012. “Bifurcations of self-excited  
666 ducted laminar premixed flames”. *Journal of Engineering for Gas Tur-  
667 bine and Power*, **134**(3), p. 031502.
- 668 [32] Heckl, M., 2013. “Analytical model of nonlinear thermo-acoustic effects  
669 in a matrix burner”. *Journal of Sound and Vibration*, **332**, pp. 4021–  
670 4036.
- 671 [33] Noiray, N., Bothien, M., and Schuermans, B., 2011. “Investigation of  
672 azimuthal staging concepts in annular gas turbines”. *Combustion Theory  
673 and Modelling*, **15**(5), pp. 585–606.



- 674 [34] Ghirardo, G., and Juniper, M. P., 2013. “Azimuthal instabilities in  
675 annular combustors: standing and spinning modes”. *Proceedings of the*  
676 *Royal Society of London A: Mathematical, Physical and Engineering*  
677 *Sciences*, **469**(2157), p. 20130232.
- 678 [35] Noiray, N., and Schuermans, B., 2013. “On the dynamic nature of az-  
679 imuthal thermoacoustic modes in annular gas turbine combustion cham-  
680 bers”. In *Proceedings of the Royal Society of London A: Mathemati-*  
681 *cal, Physical and Engineering Sciences*, Vol. 469, The Royal Society,  
682 p. 20120535.
- 683 [36] Bourgooin, J.-F., Durox, D., Moeck, J. P., Schuller, T., and Candel,  
684 S., 2015. “Characterization and modeling of a spinning thermoacoustic  
685 instability in an annular combustor equipped with multiple matrix in-  
686 jectors”. *Journal of Engineering for Gas Turbines and Power*, **137**(2),  
687 p. 021503.
- 688 [37] Parmentier, J.-F., Salas, P., Wolf, P., Staffelbach, G., Nicoud, F., and  
689 Poinso, T., 2012. “A simple analytical model to study and control  
690 azimuthal instabilities in annular combustion chambers”. *Combustion*  
691 *and Flame*, **159**(7), pp. 2374–2387.
- 692 [38] Bauerheim, M., Parmentier, J.-F., Salas, P., Nicoud, F., and Poinso,  
693 T., 2014. “An analytical model for azimuthal thermoacoustic modes in  
694 an annular chamber fed by an annular plenum”. *Combustion and Flame*,  
695 **161**(5), pp. 1374–1389.
- 696 [39] Pankiewicz, C., and Sattelmayer, T., 2003. “Time domain simulation of

- 697 combustion instabilities in annular combustors”. *Journal of Engineering*  
698 *for Gas Turbine and Power*, **125**(2), pp. 677–685.
- 699 [40] Campa, G., and Camporeale, S. M., 2014. “Prediction of the thermoacoustic  
700 combustion instabilities in practical annular combustors”. *Journal of Engineering for Gas Turbines and Power*, **136**(9), p. 091504.
- 702 [41] Staffelbach, G., Gicquel, L., Boudier, G., and Poinso, T., 2009. “Large  
703 eddy simulation of self excited azimuthal modes in annular combustors”.  
704 *Proceedings of the Combustion Institute*, **32**(2), pp. 2909 – 2916.
- 705 [42] Wolf, P., Balakrishnan, R., Staffelbach, G., Gicquel, L. Y., and Poinso, T.,  
706 2012. “Using les to study reacting flows and instabilities in annular  
707 combustion chambers”. *Flow, Turbulence and Combustion*, **88**(1-2),  
708 pp. 191–206.
- 709 [43] Poinso, T., and Veynante, D., 2001. *Theoretical and Numerical Combustion*.  
710 R. T. Edwards Incorporated.
- 711 [44] Munjal, M., 1986. *Acoustics of Ducts and Mufflers*. John Wiley & Sons.
- 712 [45] Matveev, K., 2003. “Thermoacoustic instabilities in the rijke tube: ex-  
713 periments and modeling”. PhD thesis, California Institute of Technol-  
714 ogy.
- 715 [46] Crocco, L., and Cheng, S.-I., 1956. *Theory of combustion instability in*  
716 *liquid propellant rocket motors*. Cambridge Univ Press.
- 717 [47] Goh, C. S., and Morgans, A. S., 2013. “The influence of entropy waves

- 718 on the thermoacoustic stability of a model combustor”. *Combustion*  
719 *Science and Technology*, **185**(2), pp. 249–268.
- 720 [48] Durox, D., Schuller, T., Noiray, N., and Candel, S., 2009. “Experi-  
721 mental analysis of nonlinear flame transfer functions for different flame  
722 geometries”. *Proceedings of the Combustion Institute*, **32**(1), pp. 1391  
723 – 1398.
- 724 [49] Stow, S. R., and Dowling, A. P., 2009. “A time-domain network model  
725 for nonlinear thermoacoustic oscillations”. *Journal of engineering for*  
726 *gas turbines and power*, **131**(3), p. 031502.
- 727 [50] Lehoucq, R. B., Sorensen, D. C., and Yang, C., 1998. *ARPACK*  
728 *users’ guide: solution of large-scale eigenvalue problems with implicitly*  
729 *restarted Arnoldi methods*, Vol. 6. Siam.
- 730 [51] Schuller, T., 2003. “Mécanismes de Couplage dans les Interactions  
731 Acoustique-Combustion”. Ph.D. Thesis, Ecole Central paris.
- 732 [52] Li, J., and Morgans, A. S., 2015. “Time domain simulations of nonlinear  
733 thermoacoustic behaviour in a simple combustor using a wave-based  
734 approach”. *Journal of Sound and Vibration*, **346**, pp. 345 – 360.
- 735 [53] Sensiau, C., Nicoud, F., and Poinso, T., 2008. “Thermoacoustic anal-  
736 ysis of an helicopter combustion chamber”. *AIAA paper*, *AIAA-2008-*  
737 *2947*.
- 738 [54] Wolf, P., Staffelbach, G., Gicquel, L. Y., Müller, J.-D., and Poinso, T.,  
739 2012. “Acoustic and large eddy simulation studies of azimuthal modes

740 in annular combustion chambers”. *Combustion and Flame*, **159**(11),  
741 pp. 3398–3413.

742 [55] Lieuwen, T., Torres, H., Johnson, C., and Zinn, B. T., 2001. “A mech-  
743 anism of combustion instability in lean premixed gas turbine combus-  
744 tors”. *Journal of Engineering for Gas Turbines and Power*, **123**(1),  
745 pp. 182–189.